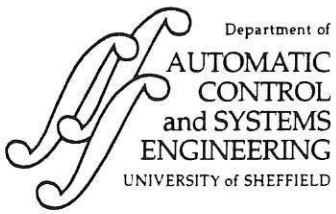

DYNAMIC CHARACTERISATION AND CONTROL OF RESONANT SWITCH MODE CONVERTERS

B Baha[1] and M O Tokhi[2]

[1] Department of Electrical and Electronic Engineering,
University of Brighton, Brighton, UK.
Email: B.Baha@Brighton.ac.uk.

[2] Department of Automatic Control and Systems Engineering,
The University of Sheffield, Mappin Street, Sheffield, S1 3JD, UK.

Tel: + 44 (0)114 282 5136.
Fax: + 44 (0)114 273 1729.
E-mail: O.Tokhi@sheffield.ac.uk.

Research Report No. 678

July 1997

Abstract

This paper presents an investigation into the dynamic modelling and control of quasi-resonant switch mode converters (QRCs). A small signal model of a QRC is derived through dynamic analysis of the system. This is used to design a controller for a zero-current switching QRC. The converter and the controller are designed, simulated and actually built. Finally, simulated and experimental results, verifying the performance of the controlled QRC in the presence of changes in load or input voltage, are presented and discussed.

Key words: *Dynamic modelling, flyback quasi-resonant converter, PI control, resonant switched mode converter, zero current switching.*

CONTENTS

LIST OF FIGURES

1 Introduction

Quasi-resonant converters (QRCs) were introduced by Liu and Lee (1985, 1986) to overcome the problems associated with the switching losses, radio frequency interference (RFI) and electromagnetic interference of pulse-width-modulated (PWM) converters at high frequency. Furthermore, the size and weight of the switching power supplies can be reduced, and the efficiency can be increased with QRCs. The resonant circuit in a QRC is formed by one additional inductor and one capacitor to shape the switching device current or voltage waveform so that sinusoidal current and voltage are generated. The active switch can be turned on or off at zero-current (ZC) or zero-voltage (ZV) switching, and hence the switching losses can be eliminated.

Despite their advantages, QCRs have not been extensively used in many industrial applications. This is because of the complexity of their circuits and the lack of suitable dynamic models and controllers. The steady-state analysis and design of different QRCs have previously been carried out by Li *et al.* (1992) and Baha (1993).

The dynamic modelling and control of QRCs, however have received little attention. A circuit-oriented analysis method has previously been suggested by Vorperian (1990) and Dijk *et al.* (1995) to obtain a dynamic model of a QRC. However, this technique does not have good theoretical support, and requires extensive knowledge of the operation of the circuit.

The output voltage of a QRC can be controlled by varying the switching frequency to compensate for changes in input voltage or load. Since PWM converters work on a constant frequency, the control methods of PWM converters cannot be directly applied to QRCs.

This paper presents a method of obtaining the dynamic model of a QRC and a novel trough current mode control method for zero-current-switching (ZCS) QRCs. The paper is organised as follows.

The dynamic modelling of QRCs is presented in Section 2. The open-loop characteristics of the converter are presented in Section 3. The design of the trough current mode controller and its compensator are presented in Sections 4 and 5 respectively.

Simulation and experimental results are given in Section 6 and finally the paper is concluded in Section 7.

2 Dynamic modelling and a flyback quasi-resonant converter

A full-wave zero-current-switched flyback QRC is chosen as an example in this section. The steady-state analysis of this converter has previously been carried out, and the corresponding d.c. voltage conversion ratio and the voltage and current stresses of the component have been obtained (Baha, 1993). The circuit diagram of a non-isolated flyback QRC is shown in Figure 1. The resonant tank (L_o and C_o) is added to shape the switch-current waveform so as to achieve zero-current switching during turn-off. The operation of the converter can be best explained by dividing the switching cycle into four distinct intervals. The equivalent circuit for each switching interval and the corresponding ideal waveforms are shown in Figures 2 and 3 respectively. The operation cycle begins at t_0 in Figure 3, and the transitions between the four different stages occur at t_1, t_2, t_3 and t_4. A full description of the operation of this converter is given in (Baha, 1993).

The standard state-space averaging (SSA) method introduced by Middlebrooke and Cuk (1976) cannot be directly used for obtaining the dynamic model of the system. This is because the resonant tank variables, which are the input variables, are changing very fast, while the low-pass filter variables are nearly constant.

In modelling dc-dc converters, the SSA method is used on the basis of the following two assumptions:

1. The switching frequency is much higher than the highest natural frequency of the converter in each switching cycle.
2. The input to the converter in each switching cycle is constant or slowly varying, as compared with the switching frequency.

The natural frequency of the resonant tank in ZCS-QRCs is greater than the switching frequency. This results in fast variation of the associated state variables. Thus, neither of

the assumptions above is satisfied. Therefore, the standard SSA method cannot be used to obtain the small-signal model of a QRC. It has also been suggested that the SSA method cannot be used to model QRCs and conventional resonant converters (Yang *et al.*, 1991). Thus, the aim of this work is to investigate an alternative method for obtaining the small-signal transfer function of QRCs. The proposed method involves obtaining the average voltage across the resonant capacitor and the average current of the resonant inductor of the QRC and using these to derive expressions for the state variables (di_L/dt and dv_C/dt) associated with the output filter. These are then used to obtain the steady-state and small-signal models of the QRC.

The following assumptions are made to analyse this circuit:

(a) The filter inductors and capacitors are larger than the resonant inductors and capacitors.

(b) The filter inductors are sufficiently large, and are treated as constant current sources.

(c) All the semiconductor devices are ideal.

(d) All *L*'s and C's are linear, time-invariant and frequency-independent.

Following a steady-state analysis (Baha, 1993), the circuit operation can be described by dividing the switching cycle into four different intervals as indicated in Figure 3. For each time interval, the following state-space equation can be written:

$$\frac{dX}{dt} = A_i X + B_i, \qquad (1)$$

where $X = \begin{bmatrix} v_C & i_L \end{bmatrix}^T$ and $i = 1,...,4$. The matrices $A_1,...,A_4$ are the state matrices and $B_1,...,B_4$ are vectors for the four switching stages. These are given as

mode-1: $$A_1 = \begin{bmatrix} -\frac{1}{RC} & \frac{1}{C} \\ -\frac{1}{L} & 0 \end{bmatrix}, \quad B_1 = \begin{bmatrix} -\frac{1}{C} i_{L_o} \\ 0 \end{bmatrix}$$

mode-2: $$A_2 = \begin{bmatrix} -\frac{1}{RC} & 0 \\ 0 & 0 \end{bmatrix}, \quad B_2 = \begin{bmatrix} 0 \\ -\frac{1}{L} v_{C_o} \end{bmatrix}$$

mode-3: $$A_3 = \begin{bmatrix} -\frac{1}{RC} & 0 \\ 0 & 0 \end{bmatrix}, \quad B_3 = \begin{bmatrix} 0 \\ \frac{1}{L} v_{C_o} \end{bmatrix}$$

mode-4: $$A_4 = \begin{bmatrix} -\frac{1}{RC} & \frac{1}{C} \\ -\frac{1}{L} & 0 \end{bmatrix}, \quad B_4 = \begin{bmatrix} 0 \\ 0 \end{bmatrix}$$

The averaged-state equation can be obtained by substituting $A_1,\ldots,A_4$ and $B_1,\ldots,B_4$ in equation (1) and simplifying as

$$\begin{bmatrix} \dot{x}_1 \\ \dot{x}_2 \end{bmatrix} = \begin{bmatrix} a_{11} & a_{12} \\ a_{21} & a_{22} \end{bmatrix} \begin{bmatrix} x_1 \\ x_2 \end{bmatrix} + \begin{bmatrix} b_1 \\ b_2 \end{bmatrix} \tag{2}$$

where,

$$\begin{aligned} a_{11} &= -\frac{1}{RC}\frac{1}{T_s}\left(T_{d1} + T_{d2} + T_{d3} + T_{d4}\right) = -\frac{1}{RC} \\ a_{12} &= \frac{1}{T_s}\frac{1}{C}\left(T_{d1} + T_{d4}\right) \\ a_{21} &= -\frac{1}{T_s}\frac{1}{L}\left(T_{d1} + T_{d4}\right) \\ a_{22} &= 0 \end{aligned} \tag{3}$$

$$\begin{aligned} b_1 &= -\frac{1}{T_s}\int_{t_0}^{t_1}\frac{1}{C} i_{L_o} dt \\ b_1 &= -\frac{1}{T_s}\frac{1}{L}\left\{\int_{t_1}^{t_2} v_{C_o} dt + \int_{t_2}^{t_3} v_{C_o} dt\right\} \end{aligned} \tag{4}$$

with T_s representing the switching period ($T_s = 1/f_s$; f_s being the switching frequency) and $T_{d1},\ldots,T_{d4}$ representing the duration of mode-1, mode-2, mode-3 and mode-4 respectively, previously discussed in (Baha, 1993).

Manipulating the expressions for b_1 and b_2 in equation (4) and substituting for $a_{11},\ldots,a_{22}$ from equation (3) into equation (2) yields

$$\begin{bmatrix} \frac{dv_C}{dt} \\ \frac{di_L}{dt} \end{bmatrix} = \begin{bmatrix} -\frac{1}{RC} & \frac{1}{C} \\ -\frac{1}{L} & 0 \end{bmatrix} \begin{bmatrix} v_C \\ i_L \end{bmatrix} + \begin{bmatrix} -\frac{1}{C}\frac{1}{2\pi}\frac{f_s}{f_0}K(i_L, v_C)i_L \\ \frac{1}{L}\frac{1}{2\pi}\frac{f_s}{f_0}K(i_L, v_C)(v_C + V_s) \end{bmatrix} \tag{5}$$

where

$$K(i_L, v_C) = \beta + \frac{Z_n i_L}{2(v_C + V_s)} + \frac{1}{Z_n i_L}(v_C + V_s)(1 - \cos\beta),$$

i_L and v_C are the state variables and

$$\omega_0 = \frac{1}{\sqrt{L_0 C_0}} = 2\pi f_0 , \quad Z_n = \sqrt{\frac{L_0}{C_0}} , \quad \beta = \sin^{-1}\left\{-\frac{Z_n i_L}{\omega C_0 (v_C + V_s)}\right\}.$$

Thus, using

$$V_1 = \frac{1}{2\pi}\frac{f_s}{f_0}K(i_L, v_C)(v_C + V_s) \tag{6}$$

$$I_1 = \frac{1}{2\pi}\frac{f_s}{f_0}K(i_L, v_C)i_L \tag{7}$$

in equation (5) yields the equivalent circuit model shown in Figure 4.

Using equations (6) and (7) and Figure 4, the derivative terms di_L/dt and dv_C/dt can be obtained as

$$\begin{aligned} \frac{di_L}{dt} &= \frac{1}{L}(-v_C + V_1) \\ \frac{dv_C}{dt} &= \frac{1}{C}\left(i_L + \frac{v_C}{R} - I_1\right) \end{aligned} \tag{8}$$

The steady-state voltage conversion ratio, v_C/V_s, can be obtained using equation (8) with $di_L/dt = 0$ or

$$\frac{di_L}{dt} = -\frac{v_C}{L} + \frac{V_1}{L} = 0$$

Thus, substituting for V_1 from equation (6) into the above, and manipulating, yields

$$\frac{v_C}{V_s} = \frac{\dfrac{K(i_L, v_C)}{2\pi}\dfrac{f_s}{f_0}}{1 - \dfrac{K(i_L, v_C)}{2\pi}\dfrac{f_s}{f_0}}. \tag{9}$$

It is noted that equation (9) is very similar to that obtained and reported previously (Baha, 1993). To perform an ac small-signal analysis, the circuit model in Figure 4 is linearised around the steady-state operating point. Small perturbations can thus be introduced into the state variables and the switching frequency as

$$\begin{aligned} i_L &= I_L + \tilde{i}_L \\ v_C &= V_C + \tilde{v}_C \\ f_s &= F_s + \tilde{f}_s \end{aligned} \tag{10}$$

where I_L, V_C and F_s represent the steady state values of i_L, v_C and f_s respectively, and $\tilde{i}_L$, $\tilde{v}_C$ and $\tilde{f}_s$ are the corresponding perturbations at the operating point.

Substituting for i_L, v_C and f_s from equation (10) into equation (5) yields

$$\frac{d\tilde{v}_C}{dt} = -\frac{1}{RC}(V_C + \tilde{v}_C) + \frac{1}{C}\left(I_L + \tilde{i}_L\right) - \frac{1}{C}\frac{1}{2\pi}K\left(I_L, \tilde{i}_L, V_C, \tilde{v}_C\right)\left(\frac{F_s + \tilde{f}_s}{f_0}\right)\left(I_L + \tilde{i}_L\right) \tag{11}$$

$$\frac{d\tilde{i}_L}{dt} = -\frac{1}{L}(V_C + \tilde{v}_C) + \frac{1}{L}\frac{\left(F_s + \tilde{f}_s\right)}{f_0}\frac{K\left(I_L, \tilde{i}_L, V_C, \tilde{v}_C\right)}{2\pi}\left(V_C + \tilde{v}_C + V_s\right) \tag{12}$$

where

$$K\left(I_L, \tilde{i}_L, V_C, \tilde{v}_C\right) = K(I_L, V_C) + \frac{\partial K(i_L, v_C)}{\partial i_L}\tilde{i}_L + \frac{\partial K(i_L, v_C)}{\partial v_C}\tilde{v}_C$$

Ignoring the second-order terms of perturbations (Vorperian, 1990), equations (11) and (12) can be linearised to yield

$$\frac{d\tilde{X}}{dt} = C\tilde{X} + D\tilde{f}_s \tag{13}$$

where

$$\tilde{X} = \begin{bmatrix} \tilde{v}_C \\ \tilde{i}_L \end{bmatrix}, \quad C = \begin{bmatrix} c_{11} & c_{12} \\ c_{21} & c_{22} \end{bmatrix}, \quad D = \begin{bmatrix} d_1 \\ d_2 \end{bmatrix},$$

$$c_{11} = -\frac{1}{RC} - \frac{1}{2\pi C}\frac{F_s}{f_0}\frac{\partial K}{\partial \tilde{v}_C} I_L, \quad c_{12} = \frac{1}{C} - \frac{1}{2\pi C}\frac{F_s}{f_0}\left(\frac{\partial K}{\partial \tilde{v}_C} I_L + K\right),$$

$$c_{21} = -\frac{1}{L} + \frac{1}{2\pi L}\frac{F_s}{f_0}\left\{\frac{\partial K}{\partial \tilde{v}_C}(V_C + V_s) + K\right\}, \quad c_{22} = \frac{1}{2\pi L}\frac{F_s}{f_0}\frac{\partial K}{\partial \tilde{v}_C}(V_C + V_s),$$

$$d_1 = \frac{K}{2\pi L}(V_C + V_s), \quad d_2 = -\frac{K}{2\pi C} I_L .$$

Taking the Laplace transform of equation (13) and setting the initial conditions to zero yields

$$s\tilde{X} = C\tilde{X} + D\tilde{f}_s \tag{14}$$

Solving equation (14) for $\tilde{X}$ yields

$$\tilde{X} = (sI - C)^{-1} D\tilde{f}_s , \tag{15}$$

where I is the identity matrix and

$$(sI - C)^{-1} = \frac{\text{adj}(sI - C)}{\det(sI - C)} .$$

Equation (15) thus gives the small-signal output-voltage-to-frequency and inductor-current-to-frequency transfer functions as

$$\frac{\tilde{v}_o}{\tilde{f}_s} = \frac{g_1 s + g_0}{a_2 s^2 + a_1 s + a_0} \tag{16}$$

and

$$\frac{\tilde{i}_L}{\tilde{f}_s} = \frac{h_1 s + h_0}{a_2 s^2 + a_1 s + a_0} , \tag{17}$$

where

$$a_2 = LC\,,\quad a_1 = \frac{L}{R} + \frac{Lf_s}{2\pi f_0}\frac{(1-\cos\alpha)}{Z_n}\left[1+\frac{(V_C+V_s)^2}{I_L^2}\right] - \frac{Lf_s}{2\pi f_0}\frac{Z_n}{2}\left[1+\frac{I_L^2}{(V_C+V_s)^2}\right],$$

$$a_0 = \frac{f_s}{2\pi RLf_0}\frac{(V_C+V_s)^2}{Z_n I_L^2}(1-\cos\alpha) + \frac{Z_n}{2} + 1 - \frac{Kf_s}{f_0} + \frac{Kf_s}{2\pi f_0}\,,$$

$$g_1 = -\frac{K}{2\pi}LI_L\,,\quad g_0 = \frac{K}{2\pi}(V_C+V_s)\left(1-\frac{Kf_s}{2\pi f_0}\right),$$

$$h_1 = \frac{K}{2\pi}C(V_C+V_s)\,,\quad h_0 = \frac{K}{2\pi}\frac{(V_C+V_s)}{R} + \frac{K}{2\pi}I_L\left(1-\frac{Kf_s}{2\pi f_0}\right).$$

Equation (16) can be used to design single-loop control with a voltage controlled oscillator (VCO). The inductor-current-to-frequency transfer function, represented by equation (17), may be used to design multi-loop controllers. In this paper, however, both equations (16) and (17) are used to obtain the relation between the inductor current and the output voltage of the flyback QRC.

Eliminating $\tilde{f}_s$ from equations (16) and (17) and simplifying yields

$$\frac{\tilde{v}_o}{\tilde{i}_L} = \frac{g_1 s + g_0}{h_1 s + h_0}\,. \tag{18}$$

Note that, as mentioned earlier, the above analyses have been carried out for ideal components. However, for the purposes of controller design, the effect of the equivalent series resistor (ESR) of the filter capacitor cannot be neglected. This introduces an additional zero in the transfer function. Hence, considering the ESR effect of the filter capacitor, equation (18) can be expressed as

$$H(s) = K_H\frac{(1-sT_{zc})(1+sT_{zesr})}{1+sT_{pc}}\,. \tag{19}$$

Equation (19) is used later in this paper to analyse and design the control circuit for the converter.

3 Open-loop characteristics

The open-loop system comprises the converter circuit modelled in Section 2. The inputs to the converter are V_s and the switching frequency f_s, and the output is V_o. The input

voltage is usually kept constant, and the output is regulated by changing the switching frequency in the presence of load changes. In the method proposed here, the output voltage of the converter is regulated by controlling the filter inductor current. Therefore, the small-signal transfer function of the output-to-the filter inductor current $H(s)$, obtained in the previous section, is considered.

The open-loop transfer function of the output-voltage-to-the filter inductor current $H(s)$ was simulated using MATLAB for low-line/heavy-load (worst-case) and high-line/ light-load conditions. The corresponding Bode plots are shown in Figures 5 and 6 respectively. These indicate that the system has low dc gain and bandwidth, thus affecting the system stability and response to certain changes. Higher dc gain and bandwidth are desirable for a stable and more robust system. Therefore, significant control action is required if the regulation of the output voltage is to be maintained.

It is noted in Figures 5 and 6 that the frequencies of the zeros and poles change considerably when the operating point of the converter changes. It is further noted that the frequency of the right-half-plane (rhp) zero is at its lowest value when the converter is operating at the worst condition (low-line/heavy-load).

To design a compensation network for the flyback QRC, the loop gain of the voltage loop has to be maximised with a suitable stability margin. However, the existence of the rhp zero in the characteristics of buck-boost derived converters limits the cross-over frequency. Therefore, the cross-over frequency is chosen well below the rhp zero frequency. Since the rhp zero moves considerably with load and input voltage, the controller is designed for the worst condition when the rhp zero frequency is low. Thus, the worst-condition value of $H(s)$ is chosen to design the controller.

4 Trough current mode control

A new control method is proposed for ZCS-QRCs and presented in this section. The method involves controlling the trough current of the filter inductor. In this method, unlike other types of current mode control for PWM converters (Ridley, 1991, Dixon, 1990, Tang

et al., 1992), the trough current of the filter inductor is controlled. A schematic diagram of the proposed control method is shown in Figure 7. The corresponding waveforms for the filter inductor current i_L, the reference current i_r and the signal controlling the switch V_{SW} are shown in Figure 8. In this method, a reference current proportional to the control voltage V_C is used to control the trough current of the filter inductor, and hence to regulate the output of the converter. Note that, when the inductor current reaches the reference current, the comparator triggers the multi-vibrator and thus turns on the active switch in the converter. The switch is kept on for a constant time, determined by the multi-vibrator circuitry, after which it turns off naturally, and the inductor current decreases. When the inductor current equals the reference current, the switch will be turned on again and the same procedure will repeat from cycle to cycle. It is noted in Figure 8 that any change in the output voltage of the converter or reference voltage V_r will introduce a change in the inductor current i_L, and will consequently change the switching frequency to regulate the output voltage of the converter.

The advantage of the proposed method over the single-loop control method is the elimination of the VCO, which is very noise-sensitive at high frequencies.

5 Compensator design

In this section a description of the design of the compensator is given. The controller is designed using the equivalent block diagram of the system shown in Figure 9, where $H(s)$ represents the output-voltage-to-filter-inductor-current transfer function of the converter given in equation (19), $G(s)$ is the transfer function of the compensator network, K_r represents the gain of the current sensing network in series with the filter inductor and K_v is the gain of the output voltage divider. The output voltage of the converter, V_o, is sensed and compared with a reference voltage, V_r, using an integrator. This results in the error voltage, V_{er}, which is fed into an error amplifier to generate the control voltage, v_C. The control voltage, in turn, programs the filter inductor current, resulting in regulation of the output voltage of the converter.

The delay in Figure 9, which is due to the switching action, introduces a further pole in the loop at very high frequencies (Dorf, 1992);

$$e^{-sT_s} \cong \frac{1 - sT_s/2}{1 + sT_s/2} .$$

This means that during half of the switching frequency the phase of the delay output decreases by 180°, whereas its magnitude remains unchanged. This extra pole will have little effect on system performance if the bandwidth of the system is below $f_s/2$. Since the bandwidth of the control system is limited to one-half of the switching frequency, the effect of the delay can be ignored, and the system can be simplified.

As indicated in Figure 8, the filter inductor current i_L can be divided into a dc part and an ac part, represented by I_1 and i_1 respectively, as shown in Figure 9. Thus, by controlling the trough current of the filter inductor, the output voltage of the converter can be regulated.

Using the block diagram in Figure 9, the output voltage can be expressed as

$$V_0 = V_r \frac{K_r G(s)H(s)}{1 + K_v K_r G(s)H(s)} + i_r \frac{H(s)}{1 + K_v K_r G(s)H(s)} \qquad (20)$$

where K_r is the gain associated with the current sensing network and K_v is the gain of the feedback resistors.

Equation (20) can be used to analyse closed-loop transfer functions as well as the noise transmission from the input to the output of the system. The transfer function $H(s)$ in Figure 8 has been obtained previously in equation (19) and the other parameters can be found from the circuit, except for the compensator transfer function $G(s)$. This has to be designed.

To obtain better dc regulation, that is a nearly zero steady-state error in the output, the compensation network must have a pole at the origin (0 Hz). To satisfy the gain characteristic of the required condition, a further pole is necessary near the ESR zero. Moreover, it is useful to introduce a zero near the cross-over frequency of the compensated system to obtain an adequate phase margin. It is noted in Figures 5 and 6 that the system

has a relatively small bandwidth. This implies that adequate regulation of the output voltage of the converter can be achieved with a PI controller. Such a controller can be realised by using an integrator incorporating two poles and a zero, so as to result in a transfer function for the compensator network as

$$G(s) = K_G \frac{1 + sT_{zg}}{s(1 + sT_{pg})} . \tag{21}$$

Using equations (19) and (21), the forward frequency response function of the compensated system in Figure 9 can be obtained as

$$T(j\omega) = K_T \frac{(1 + j\omega T_{zg})(1 - j\omega T_{zc})(1 + j\omega T_{zesr})}{j\omega(1 + j\omega T_{pg})(1 + j\omega T_{pc})} , \tag{22}$$

where $K_T = K_v K_G K_r K_H$.

6 Closed-loop performance

To study the closed-loop performance of the system, the frequencies of the pole and zero of the compensation network were chosen at $f_{pg} = 69.4$ Hz and $f_{zc} = 6.3$ kHz respectively, the values of $K_T = 82$ dB and $K_G = 91$ dB were obtained. These were used in equation (22), and the system was simulated using MATLAB. The Bode diagram of $T(s)$ thus obtained for the two conditions, that is low-line/heavy-load and high-line/light-load are shown in Figures 10 and 11 respectively.

The cross-over frequency and phase margin for the two conditions can be obtained from Figures 10 and 11. In the worst case, (heavy-load/low-line) the cross-over frequency is 3.6 kHz and the phase margin is 88°. In the case of light-load / high-line, the cross-over frequency is 4 kHz and the phase margin is 93°.

A step was then applied at the V_r input of Figure 9. The corresponding time responses of the system as obtained for the two conditions are shown in Figures 12 and 13 respectively. It is seen that the response is well damped in each case. The overshoot, as noted, is less than 10% and the rise time is about 0.4 msec. Note that the rise time is

slightly higher in the worst case and the overshoot is nearly the same in both cases. The small undershoot at the beginning of the step is due to the rhp zero.

To investigate the performance of the system under practical conditions, a 50 W flyback QRC and its controller were designed, simulated and constructed. The design procedure and steady-state-analysis of this converter has been previously outlined by Baha (1993). The circuit diagram of this converter and its control circuit are shown in Figure 14. The operation of this circuit is very similar to that shown in Figure 7, with the exception of the start-up circuit IC4 and the current-sensing network. The voltage across the filter inductor in Figure 14 is sensed and integrated to reconstruct the ac part of the filter inductor current. This signal is then summed with another signal, provided by the outer loop, to generate the control signal V_c. The control signal V_c is then compared with a fixed voltage.

Thus, when the control voltage (V_c) reaches the reference voltage, the output of the comparator will be high for a short time, and the timer will switch on the active switch in the converter. The active switch will be on for a constant time determined by R_{EXT} and C_{EXT} of the timer circuit in Figure 14. The active switch will then be turned-off naturally, and when the control signal V_c reaches the fixed reference voltage again the switch will be turned on. This operation will repeat from cycle to cycle. The method of sensing the inductor current presented in this section is different from the method presented earlier in the paper, as the inductor in the flyback QRC is formed by the magnetising inductance of the transformer and thus the filter inductor does not physically exist. Therefore, it is difficult to sense the filter inductor current directly from the inductor.

The closed-loop transient response of this practical system at low-line/heavy-load condition due to a step change in the load is shown in Figures 15 and 16. The results show a well-damped and nearly constant response under the worst conditions. The overshoot is less than 200 mV , and the settling time is about 3 msec , which is in good agreement with the simulation results, thus validating the proposed modelling and control methods. The noise appearing in the waveforms of Figures 15 and 16 is due to the ESR capacitor of the output filter. This noise may be filtered if a capacitor with low ESR is employed.

7 Conclusions and further work

An approach for dynamic modelling and control of QRCs has been proposed and validated with ZCS-QRCs under simulation and practical experimentation. With the proposed control method the minimum current of the filter inductor is controlled, and the output voltage of the QRC is regulated. A control system using flyback QRC has been analysed, designed, simulated and implemented in practice. The simulation and practical results have shown good agreement, thus verifying the proposed method of dynamic modelling and control of such systems. The main advantages of the proposed method are as follows:

1. An input-voltage feed-forward characteristic is achieved; the control circuit instantaneously changes the switching frequency if the input voltage is varied. The line regulation of the control system is excellent, and the error amplifier can be dedicated to correct the load variation exclusively.
2. The transient response is improved.
3. The dynamic analysis and control methods proposed in this paper can be extended to other QRCs and resonant converters in the range of several hundred watts up to several kilo watts.
4. The maximum value of the output current can be limited, using this control method. This will avoid the saturation problem. This characteristic can be used to control the maximum torque in a dc motor, if the power supply is used to supply the motor.

Because of low switching losses, soft switching, relatively high switching frequency operation and reduced interference of QRCs, the size and weight of power supplies can be reduced and the efficiency can be improved. Hence substantial savings, possibly of the order of 20% can be made in terms of volume and energy.

A major problem of QRCs, namely the dynamic analysis and the controller design have been solved by methods described in this paper. These converters can be used in industrial applications such as computers, communication and avionics.

Further work of interest would be to investigate the suitability of this modelling and control method for other single-output and multi-output QRCs. In particular, the dynamic analysis and control of multi-output QRCs will be important.

8 References

Baha, B. (1993). Analysis of quasi-resonant converters using the state-plane method, *International Journal of Circuit Theory and Applications*, **21**, pp. 499-512.

Dijk, E. V., Spruiji, H. N. J., O'Sullivan, D. M. and Klaassens, J. B., (1995). PWM-switch modelling of dc-dc converters, *IEEE Transactions on Power Electronics*, **10**, pp. 659-665.

Dixon, L. H. (1991). Average current mode control of switching power supplies, *Unitrode Power Supply Design Seminar handbook*, pp. 5.1-5.14.

Dorf, R. C. (1992). *Modern Control Systems*, 6th Ed., Addison-Wesley Publishing Company.

Li, J. C., Hsieh, G. C. (1992). Analysis of boost zero-current-switched quasi-square-wave converter, *IEEE Transactions on Power Electronic*, **7**, (4), pp. 673-682.

Liu, K. H. and Lee, F. C. (1985). Resonant switches - topologies and characteristics, *IEEE Power Electronics Specialist Conference Record*, pp. 106-116.

Liu, K. H. and Lee, F. C. (1986). Zero voltage switching technique in dc-dc converters, *IEEE Power Electronics Specialist Conference Record*, pp. 58-70.

Middlebrooke, R. D., and Cuk, S. (1976). A general unified approach to modeling switching converter power stages, *IEEE Power Electronics Specialist Conference Record*, pp. 18-34.

Ridley, R. B. (1991). A new continuous-time model for current-mode control, *IEEE Transactions on Power Electronics*, **6**, pp. 271-280.

Tang, W., Lee, F. C., Ridley, R. B. and Cohen, I. (1992). Charge control modelling, analysis and design, *IEEE Power Electronics Specialist Conference*, pp. 507-511.

Vorperian, V. (1990). Simplified analysis of PWM converters using the model of the PWM Switch: Parts I and II, *IEEE Transactions on Aerospace and Electronic Systems*, **26**, pp. 490-505.

Yang, E. X., Lee, F. C. and Jovanic, M. M. (1991). Small signal modelling of power electronic circuits using extended describing function Technique, *Proceedings of the VPEC seminar*, pp. 167-178.

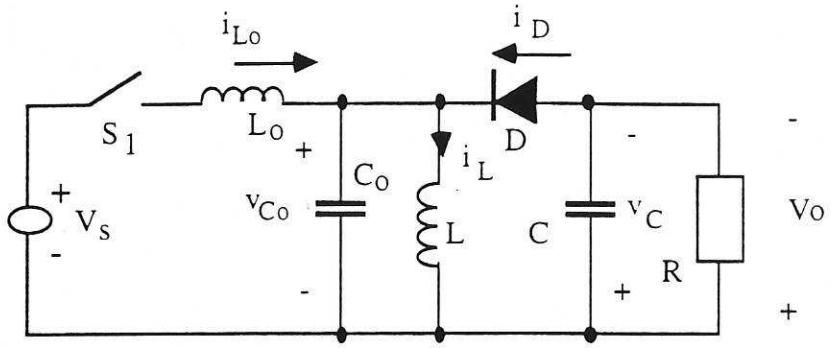

Figure 1: Non-isolated flyback QRC.

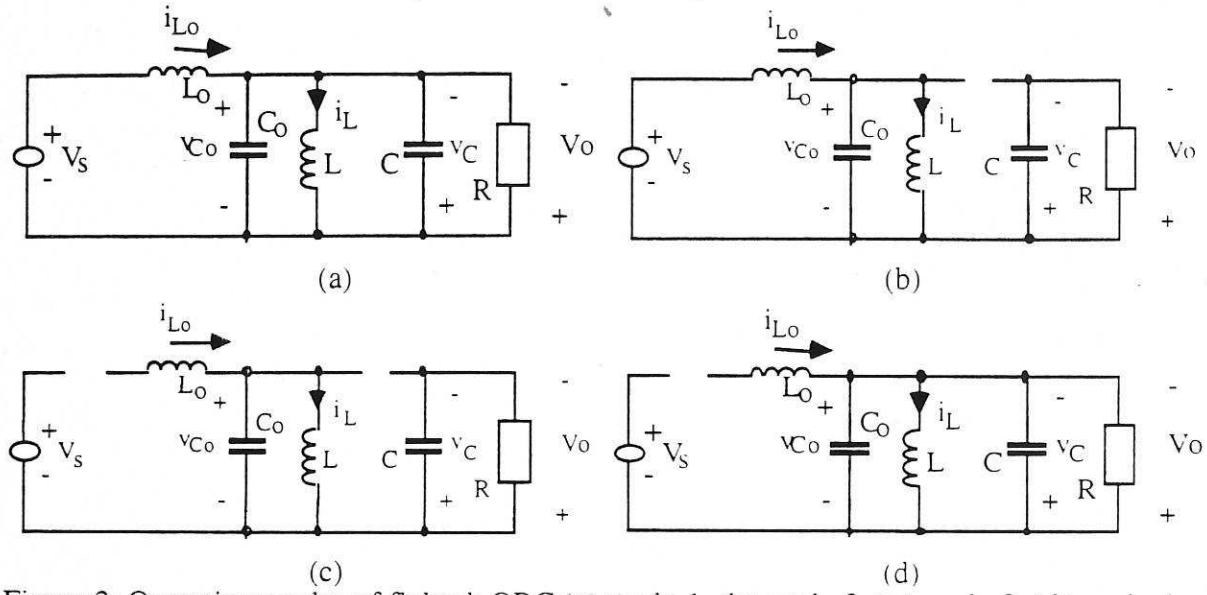

Figure 2: Operating modes of flyback QRC (a) mode-1, (b) mode-2, (c) mode-3, (d) mode-4.

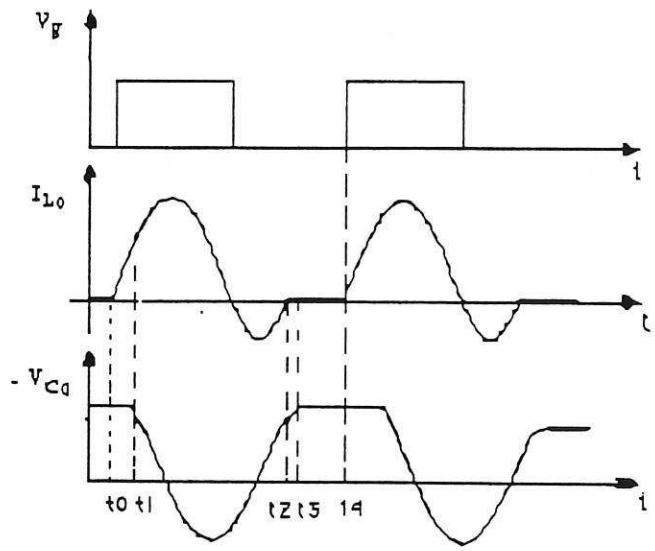

Figure 3: The waveform of flyback QRC.

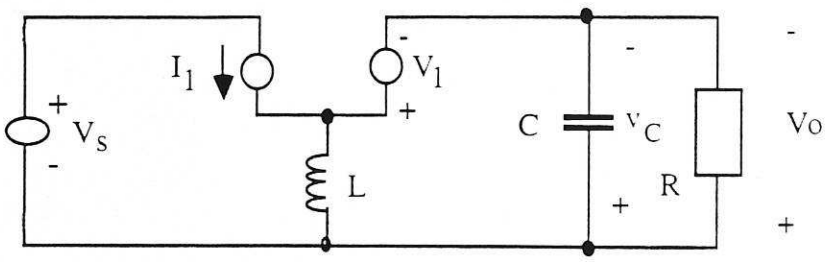

Figure 4: Average model of flyback QRC.

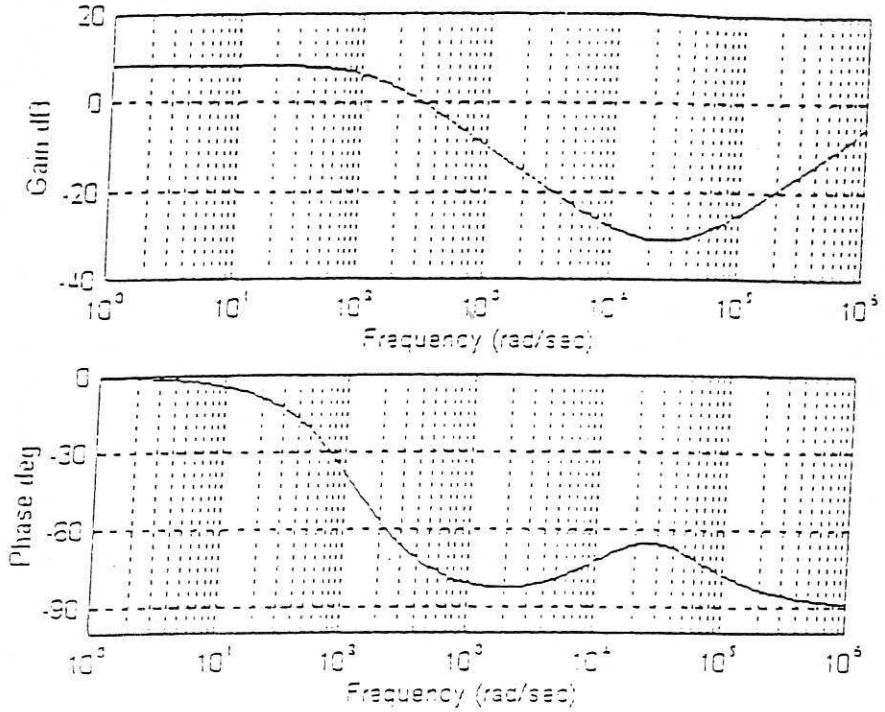

Figure 5: Bode plot of H(s) with low line and heavy load.

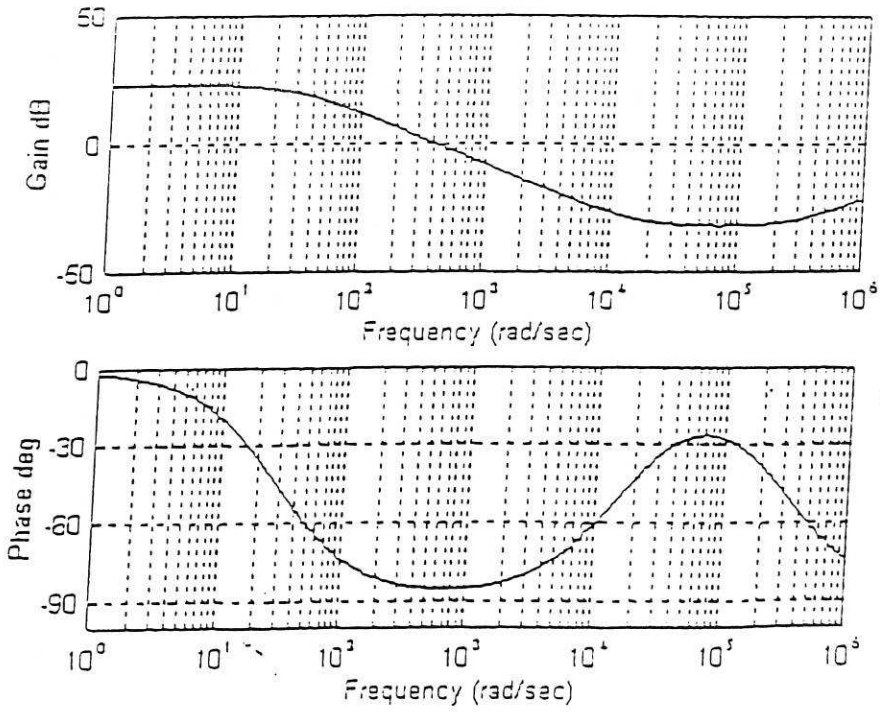

Figure 6: Bode plot of H(s) with high line and light load.

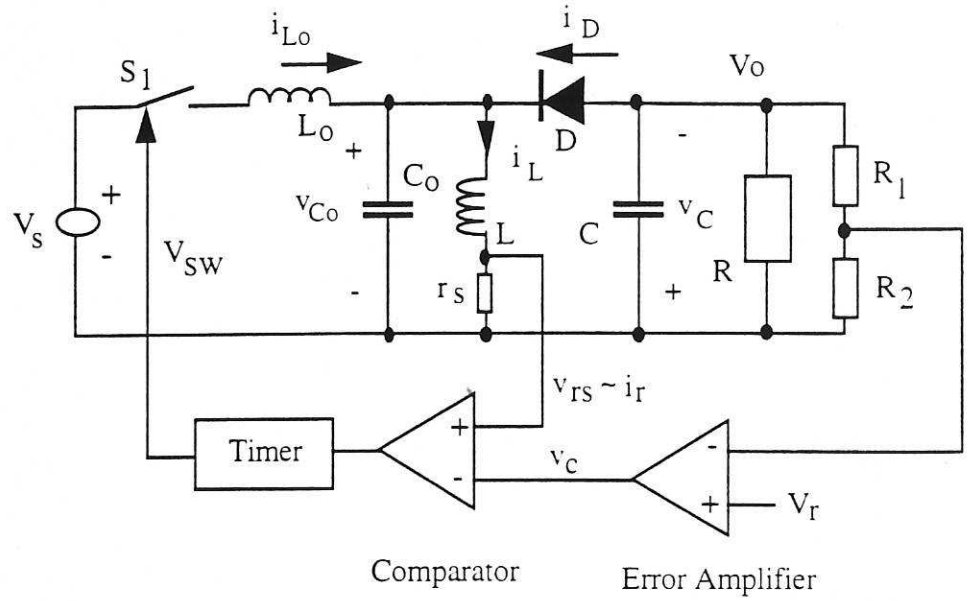

Figure 7: Schematic diagram of the proposed control method.

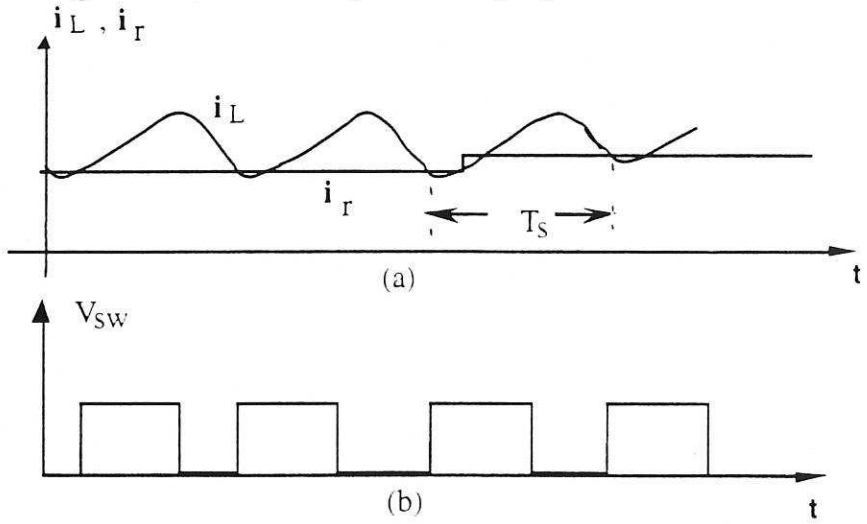

Figure 8: (a) The filter inductor current, (b) signal controlling the switch

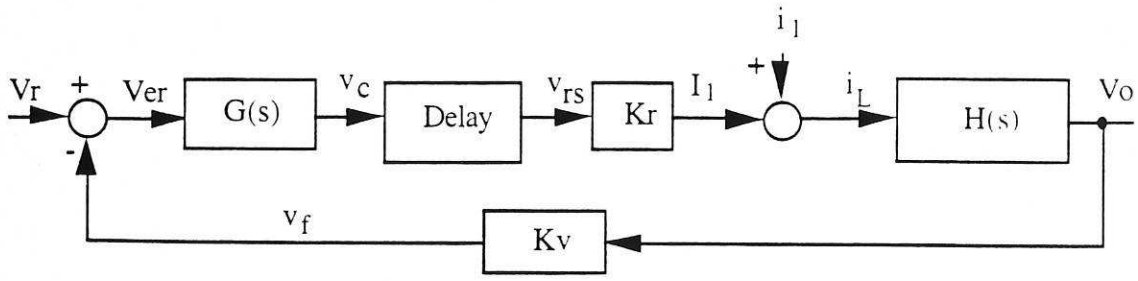

Figure 9: Equivalent block diagram of the control system.

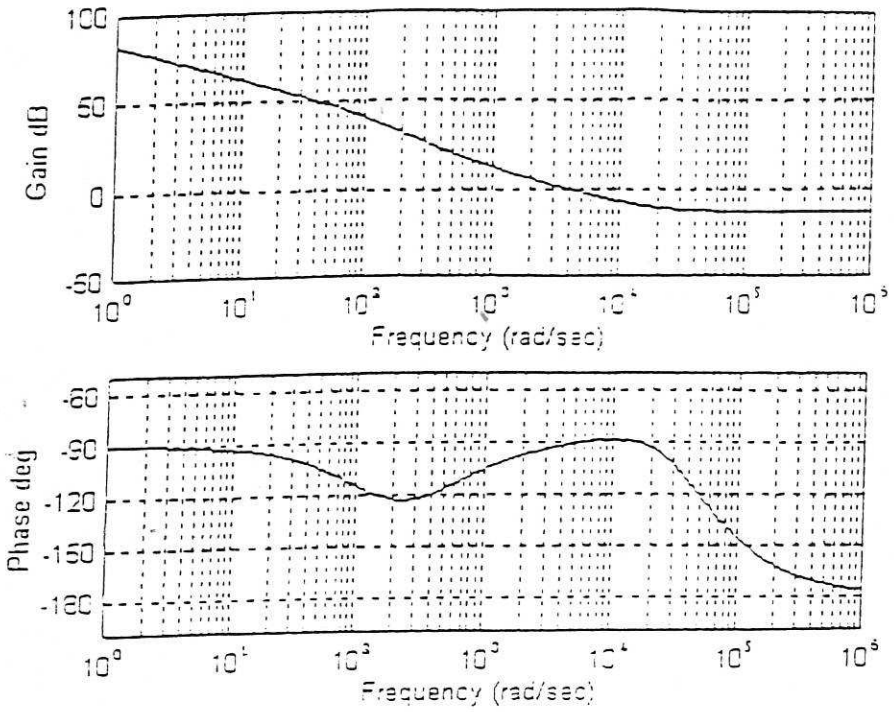

Figure 10: Bode plot of the compensated system with low line and heavy load.

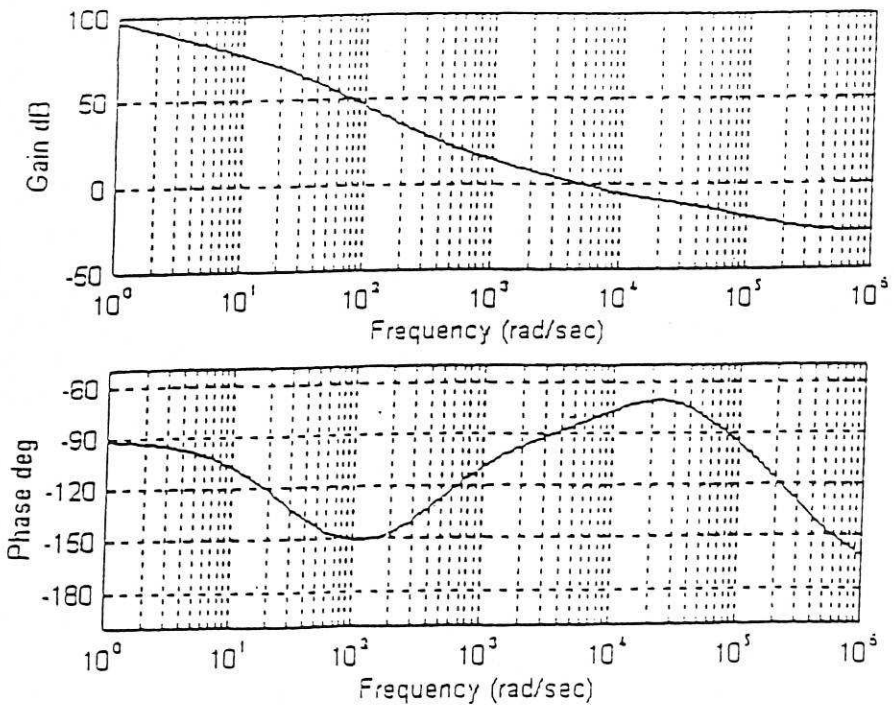

Figure 11: Bode plot of of the compensated system with high line and light load.

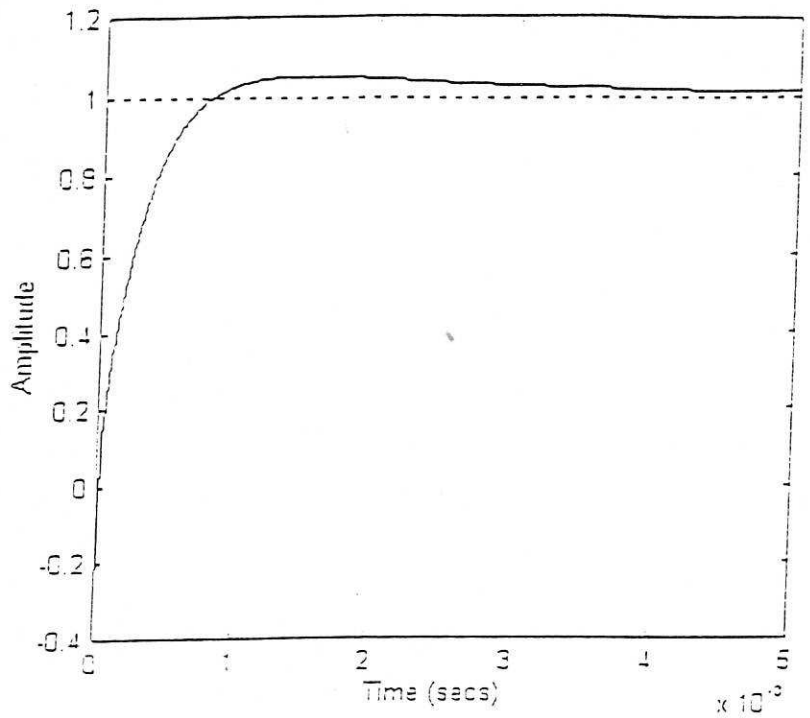

Figure 12: Simulated step response of the compensated system with heavy load and low line.

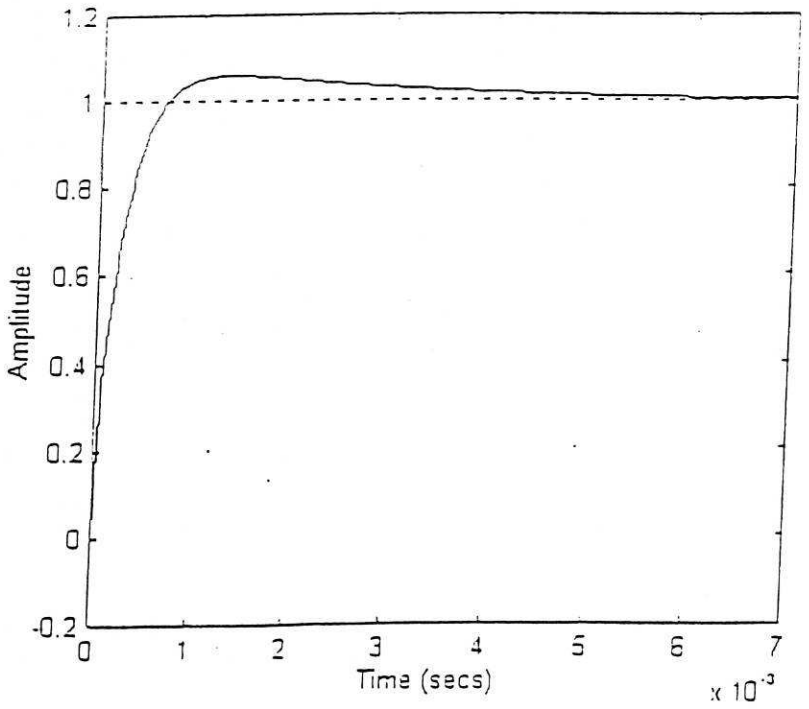

Figure 13: Simulated step response of the compensated system with light load and high line.

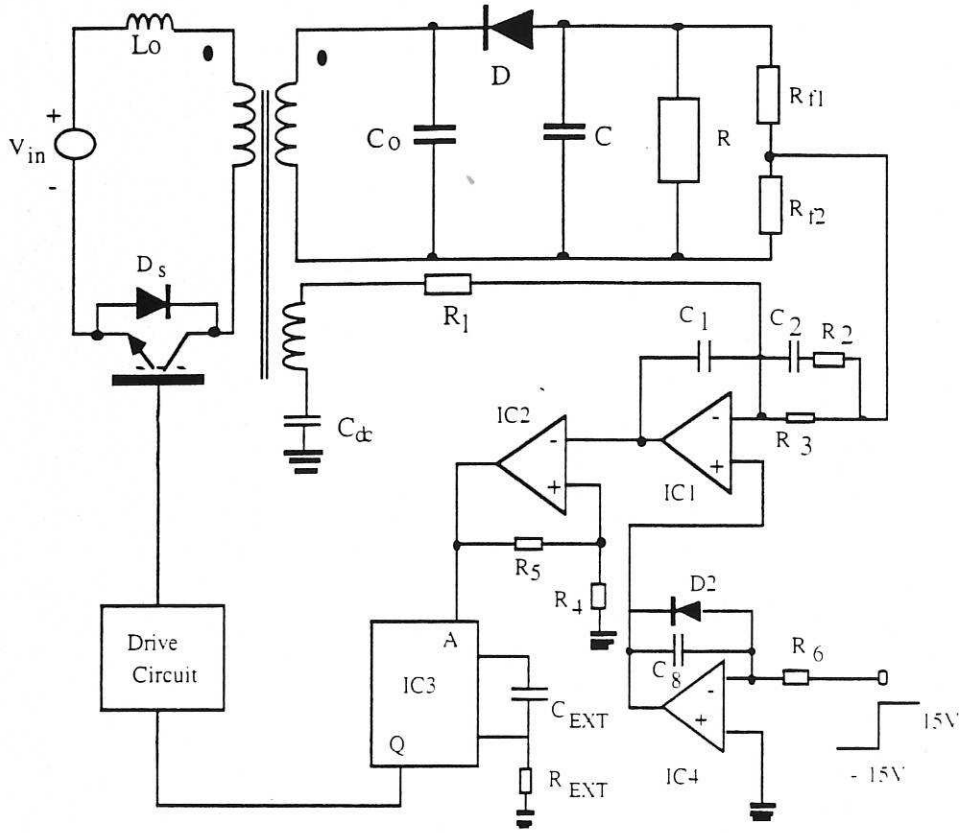

S = BUK 856-600, Ds = D =BYR-79-700, Vin = 40 - 60V , L_o = 5.8µH, C_o = 109nF, L = 88µH, C = 1200µF, R = 8Ω- 33Ω, R_{f1}= 17.3kΩ, R_{f2} = 2.7kΩ, R_1 = 18kΩ, R_2 = 300Ω, R_3 = 27kΩ, R_4 = 5.6KΩ, R_5 = 100kΩ, C_3= 1µF, C_4 = 2.2µF, C_4 = 0.2µF, R_6 = 6.8kΩ, R_{EXT} = 10kΩ, C_{EXT} = 100pF, IC1 = IC4 =LF356, IC2 = LM319, IC3 = 54LS123

Figure 14: Flyback ZCS-QRC and its controller.

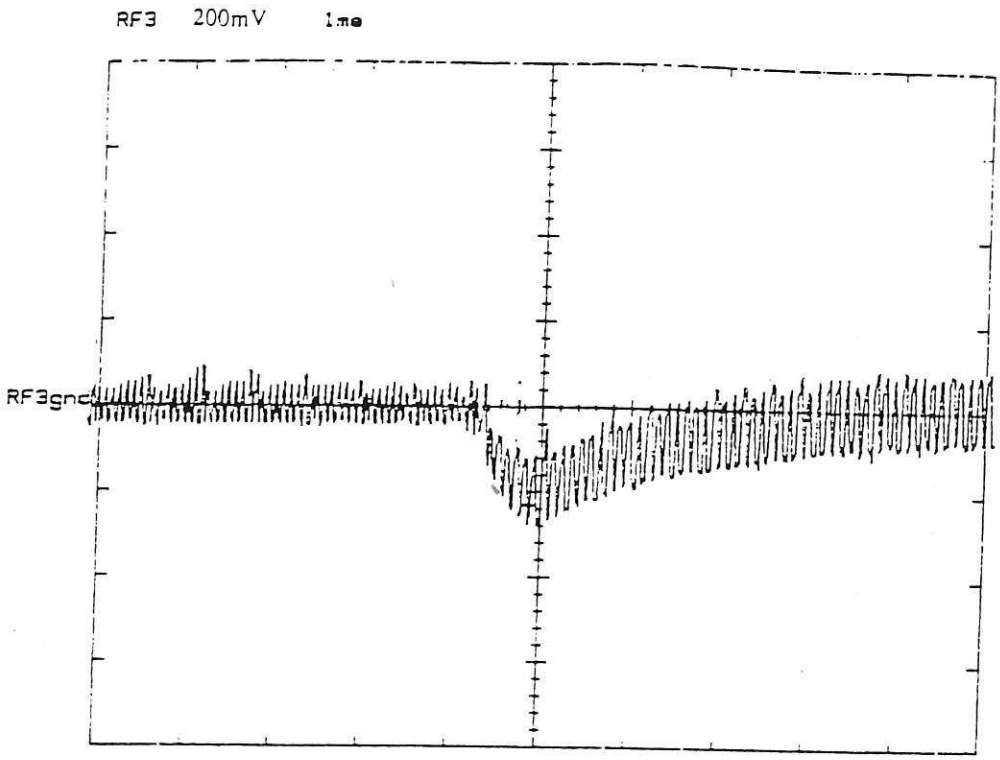

Figure 15: Measured transient response of the output voltage due to a step change in the load (20Ω - 10Ω).

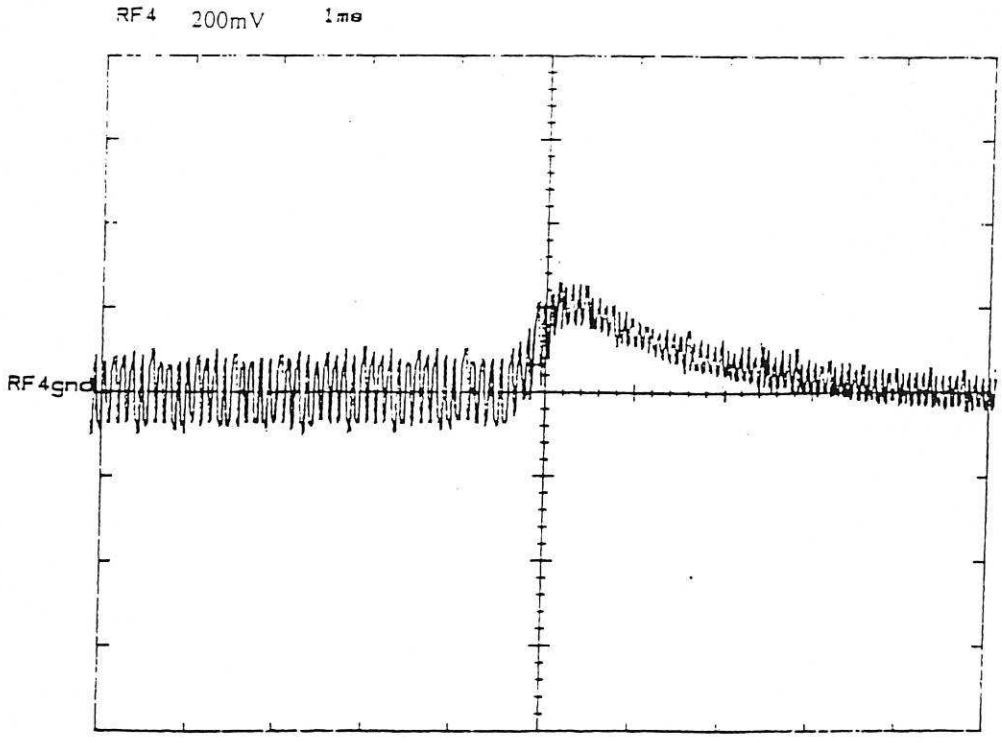

Figure 16: Measured transient response of the output voltage due to a step change in the load (10Ω - 20Ω).